VOLUME 102, Nos. 1–2   OCTOBER 2011   ISSN 0169-8095

ELSEVIER

CLOUDS · PRECIPITATION · AEROSOLS · RADIATION · WEATHER MODIFICATION

ATMOSPHERIC RESEARCH

http://www.elsevier.com/locate/atmosres

Contents lists available at ScienceDirect

Atmospheric Research

Use of Meteosat Second Generation optimal cloud analysis fields for understanding physical attributes of growing cumulus clouds

John R. Mecikalski [a,*], Philip D. Watts [b], Marianne Koenig [b]

[a] Atmospheric Science Department University of Alabama in Huntsville 320 Sparkman Drive Huntsville, Alabama 35805–1912, United States
[b] EUMETSAT European Organisation for the Exploitation of Meteorological Satellites Eumetsat–Allee 1 D-64295 Darmstadt, Germany

ARTICLE INFO

ABSTRACT

This study develops an understanding on how retrieved cloud parameter fields from the Optimal Cloud Analysis (OCA) algorithm, operating on Meteosat Second Generation (MSG), Spinning Enhanced Visible and Infrared Imager (SEVIRI) data, behave at 5-min time resolutions for growing cumulus clouds. Fields retrieved by the OCA algorithm include cloud optical thickness (τ), cloud-top particle effective radius (r_e), cloud-top pressure (p_c), and cloud-top phase. OCA is based on a one-dimensional optimal estimation methodology, and a measure of radiance fit, the cost function (J_m), is a quantity developed as part of the retrieval process and is shown to be useful in delineating mixed phase clouds; it too is evaluated (at 5-min intervals) for the information it provides.

Data for 94 growing cumulus cloud events are processed. An "event" is defined as a cumulus cloud that is monitored at 5-min intervals with OCA, as it grows from the "fair weather" or "towering cumulus" stage to near the *cumulonimbus* stage when precipitation begins. The hypothesis is that OCA products are of high-enough quality to provide unique information about microphysical processes occurring at and near cloud top. The goal through analysis of the 94 events is to identify consistent, repeating patterns in OCA fields during cloud growth that can be in turn used to infer physical processes. Data from the Convective and Orographically-induced Precipitation Study (June and July 2007) and in four regions of Europe on 25 May 2009 are used.

The validity of the OCA data is presented with a comparison to CloudSat Precipitation Radar and MODerate resolution Imaging Spectroradiometer retrieved cloud properties, showing good statistical agreements. Subsequently, results from the analysis of OCA fields for all events show that as cumuli deepen, r_e values tend to increase, and then decrease in size as cloud tops glaciate and particle settling begins. The τ magnitudes generally increase as clouds deepen, while p_c values and cloud-top temperatures fall as expected. The J_m values exhibit the pattern of spiking in magnitude (over a 5–10-min period), which indicates the increase "misfit" within OCA during the mixed phase, at about the time τ values increase substantially as clouds deepen.

© 2011 Elsevier B.V. All rights reserved.

1. Introduction

The goal of this study is to understand how satellite retrieved products designed to describe cloud properties evolve during convective cloud growth, with respect to the formation of heavy rainfall within the 1-h timeframe. It utilizes retrieved fields from the Optimal Cloud Analysis (OCA) algorithm, relying on Meteosat Second Generation (MSG) datasets as input. Four retrieved fields are analyzed at

* Corresponding author at: Atmospheric Science Department University of Alabama in Huntsville National Space Science and Technology Center 320 Sparkman Drive Huntsville, AL 35805–1912, United States. Tel.: +1 256 961 7046.
E-mail address: johnm@nsstc.uah.edu (J.R. Mecikalski).

5-min time resolution with respect to growing convective clouds: (1) cloud optical thickness (τ), (2) cloud phase, (3) effective radius of cloud-top particles (r_e), and (4) cloud-top pressure (p_c). Minimizing the "cost function" (J_m) is central to the OCA processing and a small J_m implies robust algorithm solutions; J_m is evaluated as part of this study, and will be described in detail later. Each field provides some level of unique information for this analysis. Since the cloud phase is a binary indicator (0 for water, 1 for ice) based on the other fields, our analysis will not focus on its use since analysis of τ, r_e, p_c and J_m fields provide more physical understanding.

Many previous studies describe satellite retrievals of cloud-top microphysical properties (see overviews by Arking and Childs, 1985; Rossow et al., 1985; Liou, 1992; Kidder and Vonder Haar, 1995); these retrievals have used data from the Geostationary Operational Environmental Satellites (GOES; Strabala et al., 1994; Min and Harrison, 1996; Greenwald and Christopher, 2000; Lindsey and Grasso, 2008; Smith et al., 2008; Heidinger and Pavolonis, 2009); the MODerate Resolution Imaging Spectroradiometer (MODIS; King et al., 1998; Baum et al., 2000a,b,c; Dong et al., 2008; Minnis et al., 2008; Yuan et al., 2008; Menzel et al., 2010, to name a few); the Advanced Spaceborne Thermal Emission and Reflection Radiometer (ASTER; e.g., Hulley and Hook, 2008); and the Advanced Very High Resolution Radiometer (AVHRR; Parol et al., 1991; Baum et al., 1992; Nakajima and Nakajima, 1995; Hutchison et al., 1997; Pavolonis and Heidinger, 2004; Pavolonis et al., 2005; Zhao et al., 2008). The theoretical studies of Nakajima and King (1990) and Menzel et al. (2010) have served as guidance for the development of cloud-top retrieval algorithms and typing methodologies.

The main reasons for retrieving cloud properties from satellite include enhancing understanding of radiative forcing impacts on climate (Minnis et al., 1998, 1999, 2004a; Dong et al., 2005, 2006; Yuan et al., 2008), verifying convective parameterization methodologies and assessing convective storm behavior (Lindsey et al., 2006; Rosenfeld et al., 2008; Fan et al., 2009), and increasing understanding of the atmosphere as a whole with respect to clouds (Duda et al., 2001; Lopez et al., 2009). Time series analysis of retrieved τ, r_e, cloud phase and p_c have been evaluated on scene-by-scene time scales from AVHRR in the evaluation of clouds with respect to climatological datasets like those for the International Satellite Cloud Climatology Project (ISCCP; Rossow and Schiffer, 1991, 1999). Cloud property retrievals from GOES have been used in aviation applications related to icing (Smith et al., 2000; Dong et al., 2002; Smith et al., 2002, 2003; Minnis et al., 2004b), and for enhancing numerical weather prediction models (Weygandt et al., 2006).

The study by Duda et al. (2004) focuses beyond the analysis of retrievals from single-images, considering the time trends of these data as a cloud grows and evolves. However, no studies to date attempt to assess *high-temporal* (5-min) resolution changes in retrieved cloud-top properties, in this case with respect to rapidly evolving cumulus clouds in advance of producing rainfall at the ground. Cumulus clouds prior to generating rainfall and lightning undergo rapid changes, often possessing internal updrafts >20 ms^{-1}, and therefore grow through several kilometers of atmosphere within 5–30 min. Cloud-top properties for convective clouds, as viewed by geostationary satellites such as MSG or GOES, will therefore change quickly, on time scales of 5 min or less. Monitoring these changes using OCA-retrieved microphysical fields is hypothesized to help address diagnostic and predictability issues related to in-cloud updraft magnitude (which influence r_e as a function of time), cloud-depth increases, inferred storm intensity (in terms of rainfall and severe weather parameters), ground-level winds, lightning flash rates and perhaps microburst potential. Rosenfeld et al. (2008) have demonstrated some forecast skill between cloud-top r_e for liquid drops and tornado occurrence (in a relative sense related to surrounding storms). For this study, we wish to determine relationships between OCA fields and patterns in advance of convective initiation (CI), as defined here as the first occurrence of a ≥ 35 dBZ radar echo from a new cumulus cloud within the 0–1 h timeframe from present (e.g., Schreiber, 1986; Wilson and Mueller, 1993).

Therefore, the main goal of this study is to understand how OCA retrieved fields for growing convective clouds, at 5-min temporal resolution, may be used to understand in-cloud processes related to physical aspects of cumulus cloud growth, which include updraft strength and phase changes related to r_e changes, τ as a function of cloud depth, and cloud longevity. Identifying these interactions will help extend our understanding of cloud-top–in-cloud relationships, to promote the use of OCA (or OCA-like) products for convective cloud diagnosis, and to eventually incorporate retrieved microphysical fields within algorithms that nowcast (0–1 h forecast) new thunderstorm formation or intensity.

Section 2 of this paper provides background on the OCA algorithm and its data, as well as methods for inferring physical aspects of growing cumulus clouds in geostationary satellite data. Section 3 describes the processing methodology. OCA product quality is demonstrated in Section 4, and finally, the study's main results, and conclusions are discussed and presented, in Sections 5 and 6, respectively.

2. Background and data

2.1. Spinning Enhanced Visible and Infrared Imager (SEVIRI) data

The main data for this project, as used in the OCA retrieval algorithm, are 5-min, calibrated Level 1.5 visible (VIS) and infrared (IR) channel data collected by the SEVIRI instrument on the MSG-1 (*Meteosat-8*) and MSG-2 (*Meteosat-9*) satellites, as located over the Equator at 9.5° and 0° longitude, respectively. *Meteosat-9* data were available at 5-min resolution during the Convective and Orographically-induced Precipitation Study (COPS; Wulfmeyer et al., 2008) in 2007. The sub-satellite sampling distance is 3 km, while data resolution over Europe and the domain of COPS 2007 is >3 km due to view angle (the location where data were collected and processed). The SEVIRI instrument possesses 8 IR channels, having central wavelengths of 3.9, 6.2, 7.3, 8.7, 9.7, 10.8, 12.0 and 13.4 μm, one near-IR 1.6 μm reflectance channel, two VIS channels centered on 0.6 and 0.8 μm, and one high-resolution VIS channel (HRV; Schmetz et al., 2002). [See also European Organisation for the Exploitation of Meteorological Satellites (EUMETSAT), 2007a.]

2.2. Cloud physical parameter retrievals and OCA

The unique aspects of this study are that cloud properties are analyzed on high-temporal frequency scales (5 min) for growing convective clouds; data at this time frequency is a property of *Meteosat-8/-9* over Europe, and will be on other forthcoming geostationary satellites. Here, "growing" implies a convective cloud with a sustained updraft that will develop to produce substantial rainfall (≥ 35 dBZ echo intensity). Monitoring cloud-top properties can imply several aspects of convective clouds as related to the near-term (0–1 h) behavior of the convective storm that may follow. These include: (1) particle size (measured in terms of r_e) as related to in-cloud updraft strength (Rosenfeld et al., 2008, for liquid drops) and cloud-top temperature, (2) r_e as related to cloud base altitude, aerosols and relative humidity of the updraft (Lindsey et al., 2006, 2010), (3) τ changes related to increases in cumulus cloud depth, (4) changes in r_e as a function of cloud-top phase changes (i.e. the glaciation process), and (5) r_e changes as clouds age and ice particle settling occurs. Due to a lack of information, we will not address relationships between OCA fields and aerosols, which influence τ and r_e. We will address the other aspects through analysis of 94 growing convective cloud events. Retrieved OCA fields from the COPS experiment domain over southern Germany and northeastern France, as well as over four regions in central Europe on 25 May 2009, are analyzed to address these science questions.

The OCA algorithm is fully described in Watts et al. (1998) and Poulsen et al. (in press). For the purposes of this paper, the main aspects of OCA are described, focusing on the optimization, main assumptions, use of background (numerical weather prediction, NWP) model or environmental fields, and the data used within OCA to obtain specific fields. The basic state vector of the retrieval is

$$\mathbf{x} = [\tau, r_e, p_c, f, T_s] \qquad (1)$$

[units (unitless, μm, hPa, unitless, K)], where f is the cloud fraction, and T_s is surface skin temperature. Although clearly not a "cloud" parameter, T_s is included in the retrieval because of its potentially large effect on IR radiances that sometimes (when poorly forecasted over land with low cloud fraction or thin clouds) leads to poor retrievals. The measurement vector identifies the SEVIRI channels used within OCA, and is given as $\mathbf{y} = [0.6, 0.8, 1.6, 6.2, 7.3, 8.7, 10.8, 12.0, 13.4]$ μm. The 0.6, 0.8 and 1.6 μm channels are in percent reflectance (0–1), whereas the other channels are brightness temperatures (T_B; K). As presented later, $\mathbf{y(x,b)}$ is a measurement vector resulting from the OCA fast radiative transfer model operating on a state $\mathbf{x}$ and fixed model parameters $\mathbf{b}$, and $\mathbf{y_m}$ is a vector of actual measurement data.

As the basic principal of optimal estimation, the method for retrieving OCA fields, is to maximize the probability (P) of the retrieved state conditional on the value of the measurements and any *a priori* information, it is required to maximize $P(\mathbf{x|y, x_b, b})$. Here, $\mathbf{x_b}$ is the prior value of $\mathbf{x}$, and $\mathbf{b}$ includes all other elements of the forward model. Vector $\mathbf{b}$ includes NWP humidity $[\mathbf{H(z)}]$ and temperature profiles $[\mathbf{T(z)}]$, surface albedo and emissivity at the IR channel wavelengths ($\boldsymbol{\varepsilon}$), and other spectroscopic and scattering (refractive index) infor-

mation. Therefore, $\mathbf{b} = [\mathbf{H(z)}, \mathbf{T(z)}, \mathbf{R_s}, \boldsymbol{\varepsilon}]$, where $\mathbf{R_s}$ is a vector of surface reflectance at 0.6, 0.8 and 1.6 μm. The problem then is toward maximizing $P(\mathbf{x|y}, \mathbf{x_b}, \mathbf{b})$ for given values of $\mathbf{y}$, $\mathbf{x_b}$ and $\mathbf{b}$.

Minimizing the negative logarithm of P is equivalent to maximizing the probability, and hence we want to minimize J with respect to $\mathbf{x}$, where J is written as

$$J = [\mathbf{y(x)}-\mathbf{y_m}]\mathbf{S_y^{-1}}[\mathbf{y(x)}-\mathbf{y_m}]^T + (\mathbf{x}-\mathbf{x_b})\mathbf{S_x^{-1}}(\mathbf{x}-\mathbf{x_b})^T + (\mathbf{b_t}-\mathbf{b})\mathbf{S_b^{-1}}(\mathbf{b_t}-\mathbf{b})^T \quad (2)$$

In Eq. (2), $\mathbf{S_y}$ is the error covariance of the measurements, $\mathbf{S_x}$ is the error covariance of the *a priori* state, and $\mathbf{S_b}$ is the error covariance of the forward model parameters, and the three terms then represent the weighed deviations from measurements, the *a priori* state, and the model parameters, respectively. Vector $\mathbf{b_t}$ is the unknown true value of the model parameters. The derivative of J is independent of the last term in Eq. (2) involving the model parameters, and it therefore disappears from the subsequent analysis.

The error covariance matrices $\mathbf{S_y}$ and $\mathbf{S_x}$ (the quality of the measurements and prior state) provide statistical constraints on the solution. The information available in the prior state is limited. For the pure cloud parameters τ, r_e and p_c there is effectively no information other than broad climatology and, to avoid biasing retrievals to some arbitrary center value (e.g. 500 hPa for p_c), the variances for these are set effectively to ∞. For f in Eq. (1), we have prior information from the cloud mask (EUMETSAT, 2007b), yet it is in the form of a binary switch: fully cloudy or cloud-free. Although it could be argued that the prior f should be 1.0 with a small error (as only cloudy pixels are considered), in practice this leads to somewhat arbitrary trade-offs between f, τ and p_c even when f is clearly unity. Therefore in the current OCA, the variance is set to zero implying a perfect knowledge that the pixel is completely cloud covered. The retrieved f will always be 1.0, and where it is actually not, in cloud edge pixels, the other parameters, τ and p_c, will compensate. The variance for T_s is set as $(1.0)^2$ or $(6.0)^2$ K^2 according to whether the pixel is over land or sea, respectively, reflecting the relative accuracies of forecasts of T_s. All prior estimate errors are assumed uncorrelated (off-diagonal terms of $\mathbf{S_x} = 0$).

A very important output diagnostic of OCA is the cost function J itself at the solution (i.e. effectively the last calculated value of the minimization). In practice, and especially as the prior information is weak, only the measurement part J_m (i.e. $J \approx J_m$), the first right-hand side term, Eq. (2) is used. As the OCA implementation uses significantly more measurement channels (9) than there are independent state variables (~3), a perfect fit to the measurements at the solution is not possible. The fit becomes worse as the cloud scene departs from the assumed simple (plane-parallel) model. Pixels with gross model departures like multiple layer cloud result in a high cost, and these can therefore either be ignored or potentially treated in a different way. Other model departures that can lead to high solution J_m include, for example, shadowing, grossly incorrect surface albedos (e.g. un-modeled sea ice), sun glint etc. The diagnostic is not perfect; an empirical threshold must be set, the plane-parallel model can accommodate some model departures, and finally a high cost does not indicate *what* the problem is, only that there is one. One aspect of this study is to determine whether J_m alone provides valuable information on

cloud processes, despite being a parameter not directly related to cloud dynamics.

3. Processing methodology

This study's methodology follows directly from Mecikalski et al. (2010a,b) in how growing convective cloud events were identified. *Meteosat-8/-9* data used in the study were, in part, collected for 50 growing cumulus cloud events observed during four particularly active convective weather days in June and July 2007 during COPS (www.cops2007.de). The geographical domain over which data were processed was 6.5–11.0° E, 46.5–49.0° N. CI events occurring in conditions not obscured by higher clouds were sought, i.e. new cumulus could be easily observed by *Meteosat-8/-9*. To complete the dataset, it was more efficient to process data in other highly convectively active locations (not during COPS). Therefore, data for 44 CI events were also collected over four portions of central Europe on 25 May 2009: (1) central Italy, (2) the eastern Alps Mountains, (3) northern Spain, and (4) northwestern France. Table 1 presents the case days analyzed, the times on each day over which data were collected, and the number of storms specifically identified.

A "good quality" event is defined as cumulus clouds developing in mostly clear–sky conditions over a 30-min time period preceding in which new cumulus clouds were observed, then 15–45 min into the future without "interference" from high-level cirrus as *cumulonimbus* clouds evolved with anvils. High-level cirrus at the cumulus cloud stage often leads to false identification as cloud typing is difficult to determine. For all days and locations, imagery was gathered, and subset domains of 131 elements by 61 lines in the IR (393 × 183 HRV) were analyzed from Northern Hemispheric data.

The method of convective cell tracking involved manually observing towering cumuli that evolved over six successive 5-min images into a large cumulus cloud (*cumulus congestus* and *cumulonimbus*), or a cloud that clearly possessed a new cirrus cloud anvil. Comparison to radar datasets from the COPS campaign (e.g. POLDIRAD), and over the four regions, was done to confirm the eventual occurrence of a ≥ 35 dBZ echo, between 15 and 45 min after the 30-min period each cloud was analyzed (i.e. 15–45 min after the "0 min" point). For the 94 growing cumulus cloud cases listed in Table 1, OCA fields were gathered for a 3 × 3 pixel region centered over the growing cloud, with the *coldest three pixels* (as determined from the 10.8 μm channel) averaged to comprise the results.

Table 1
List of growing cumulus cloud events studied, along with the date and location the events were collected and processed. See Fig. 1 for specific locations for data used on 25 May 2009.

(See Fig. 10)	Date and location	Number of events
a	4 June 2007 COPS Region	12
b	5 June 2007 COPS Region	13
c	8 June 2007 COPS Region	15
d	20 July 2007 COPS Region	10
e	25 May 2009 Central Italy	10
f	25 May 2009 Eastern Alps	15
g	25 May 2009 Northern Spain	11
h	25 May 2009 Northwestern France	8

4. OCA field quality

Watts et al. (1998) briefly describe the validation of OCA, with much validation subsequently being done using data from the National Aeronautics and Space Administration "A-Train" constellation. Specifically, retrieved cloud-top properties from MODIS and the CloudSat Precipitation Radar (CPR) have been compared to OCA fields, τ, r_e, and p_c. MODIS products are obtained from the MAC06S1 dataset, while the CPR data are from the 2B-GEOPROF (cloud mask and radar reflectivity) and 2B-CLDCLASS products.

As a means of demonstrating field quality, validation of the OCA products is done here as SEVIRI data coincident with 12 daytime overpasses of the A-Train constellation between August 2006 and June 2008 are analyzed (Fig. 2a). Fig. 3 shows a comparison of the CPR and OCA p_c where the values are filtered using the OCA quality control threshold $J_m < 90$, which implies uniform cloud types (complete stratus, cirrus or cumulus cover) over 3 km² SEVIRI pixels. Retrievals with J_m values ≥ 90 are avoided in this validation exercises simply because the quality of the retrieval is considered low, and hence the comparisons are less easy to understand. High J_m values imply mixed cloud scenes, specifically cirrus overlying stratus, or multi-layer clouds. Hence, in the growing cumulus cloud analysis to follow, pixels with J_m values much larger than 90 are used to infer mixed phase cumulus clouds.

Applying this $J_m < 90$ quality check for this validation step only eliminates 44% of the total ~14 600 pixels, for all cloud types (stratus, cirrus, cumulus, mid-level clouds). Apart from some occurrences of low OCA values (probably from marginal multi-layer situations that escape the quality control check) the distribution is clean with a correlation of 0.91, bias of + 0.89 km (OCA low), and a standard deviation of 1.68 km. The bias appears smaller for clouds below 5 km probably as these are mainly optically dense water clouds.

The r_e and τ validation must currently be made against MODIS derived values which, subject to many of the same modeling limitations and assumptions, do not provide such a robust validation source as is available for p_c. When the cloud conditions are more straightforward (i.e. single-layered), as in the data from an overpass containing exclusively strato-cumulus scenes over the Southern Atlantic Ocean (Fig. 2b), there is a good coherence between the OCA and MODIS products (Figs. 4 and 5). Correlations of 0.91 and 0.71 for τ and r_e, respectively, as well as small biases −0.28 for τ and −0.18 for r_e, are found. Standard deviations are 3.58 for τ and 2.47 μm for r_e.

For a larger 12-orbit sample of overpasses (Fig. 2a), the OCA–MODIS coherence is significantly lower (Fig. 6). In τ (11 118 pixels), the correlation decreases to 0.61 and the standard deviation ~11.0, as compared to 0.91 and 3.58 for the stratocumulus. The bias remains reasonably low at + 1.35[1]. Similarly, Fig. 7 shows 10 037 pixels for the same dataset in Fig. 6, where the r_e correlation is reduced to 0.63 (0.71 for stratocumulus) and the standard deviation 6.5 μm (2.47 μm). One significant feature of the r_e comparison is the deviation for

---

[1] Too much significance should not be attached to the low bias as refinements to the SEVIRI VIS channel calibrations have been made with reference to MODIS VIS data.
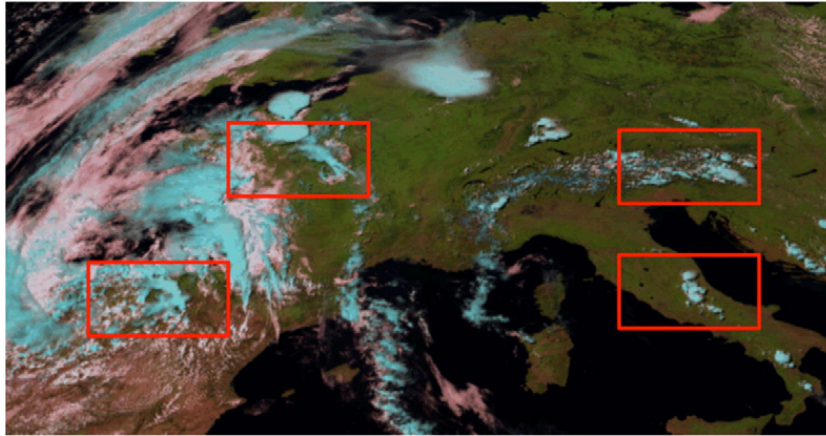
Fig. 1. Domains on 25 May 2009 used for 5-min OCA field analysis of growing cumulus clouds. The number of events per domain is listed in Table 1.

larger values, where the MODIS r_e rarely rise above 30 μm. This deviation is likely related to differing assumptions for the scattering and microphysical models for ice clouds. Otherwise, we may suppose that, when including inhomogeneous (non-stratus type) clouds, the comparisons show genuine retrieval problems related to non-plane-parallel solar illumination and assumptions of scene homogeneity in the retrieval, and more artificial problems related to sampling volumes (the MODIS nadir field-of-view is ~1 km compared to the SEVIRI oblique field-of-view of 3 to 6 km).

Results for pixels (with CPR cloud-top heights in the 2–8 km range; not shown), over the 12 orbits shown in Fig. 2a, demonstrate lesser reliability in the OCA fields for clouds with mixed phase cloud-top characteristics. Correlation coefficients for τ and cloud-top height (p_c) fields are 0.49 and 0.83, respectively, with standard deviations being 13.30 and 1.13 km. Correlation values of r_e for ice and water clouds are 0.34 and 0.38, respectively. These lower values suggest difficulty in OCA for discerning r_e information for clouds near the freezing altitude. With respect to the present study, despite these errors for clouds within the cumulus height range, since the results below focus on the relative changes in

τ and r_e as cumulus clouds grow, and not the absolute values, it is felt that solid conclusions can be developed from these OCA data.

5. Results

Following the physical relationships discussed earlier, and given the high-quality of the retrieved OCA parameters, several main questions are addressed: (1) What are the behaviors of the OCA fields (phase, τ, p_c, r_e, J_m) as clouds evolved over 30-min intervals as cumulus clouds? (2) What are the relationships between 5 to 30 min rates of change of OCA fields and other IR indicators that infer physical processes in growing cumulus (cloud depth and updraft strength)? (3) Are τ time change rates valuable indicators of cloud evolution? (4) Can J_m be used as an early indicator of cloud-top glaciation? Specifically, does an increasing J_m imply the beginning of the mixed phase at cloud top? Over the following two sections these questions will be addressed as the 94 events are examined. An example of the spatial patterns of the τ, r_e and p_c fields is shown for 1320 UTC 25
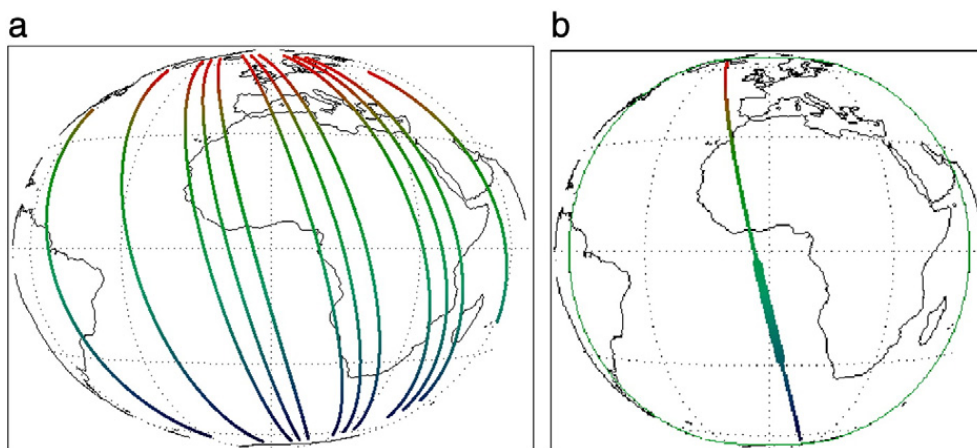

Fig. 2. (a) Paths for 12 daytime NASA A-Train orbits from August 2006 to June 2008, as used in the OCA validation (Figs. 3–7). Orbits were chosen as they each contain at least some examples of multi-layer cloud. In (b), the A-Train orbit from which these data were collected, with the stratocumulus section being highlighted by a thick line (28.2° S, 3.1° E to 2.9° S, 2.6° W).
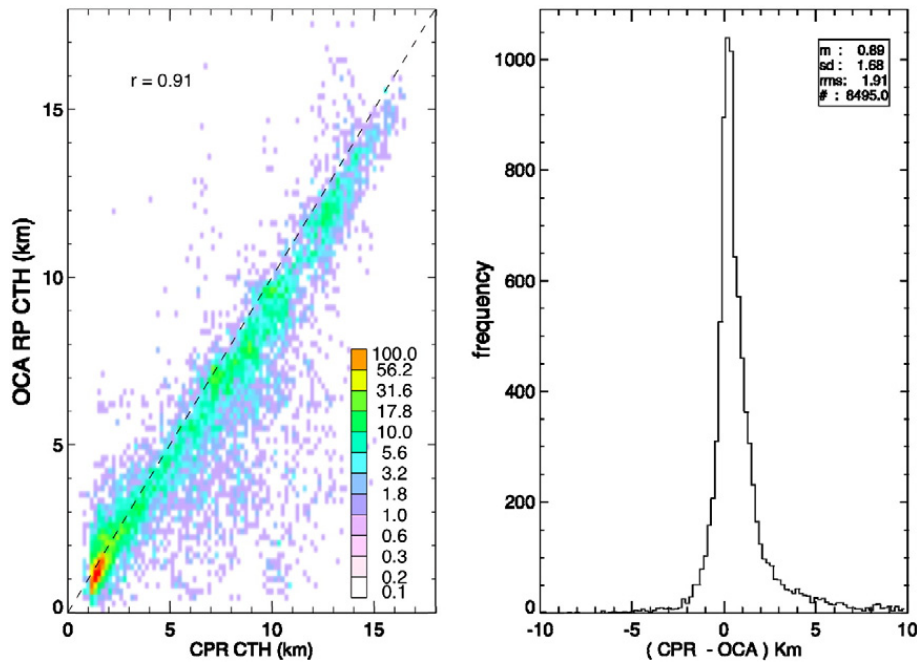
Fig. 3. Log density scatter plot of CloudSat Precipitation Radar (CPR) and OCA cloud-top height (CTH, km; for validation of cloud-top pressure, p_c; left), and histogram of differences (right), for 12 daytime A-Train orbits from August 2006 to June 2008 (as shown in Fig. 2a), for a total of 8493 pixels. OCA data is quality controlled with $J_m \leq 90$. See text for discussion.

May 2009 over a large section of Europe in Fig. 8(b–d), with an accompanying true color image shown in Fig. 8a.

5.1. OCA field evolution

Fig. 9(a–h) presents the time-trended OCA fields for all storms for the eight days and regions analyzed. Per-storm results are presented in Fig. 10(a–d) in Section 5.2. In Figs. 9 and 10, the abscissa spans 30 min, −30 to 0. The 0-min point is the time when the cumulus clouds are deepest, and likely 15–45 min before rainfall of significant intensity (>30–35 dBZ) would begin reaching the ground, i.e. CI. The ordinate is scaled 0–120, representing units of four fields: p_c in kPa decreases downward (i.e. downward is higher cloud tops), while τ (unitless), J_m (plotted as $J_m \div 10$; see right-hand scale), and r_e (μm) all increase upward. J_m is divided by 10 for display purposes to help reduce the large variability in this quantity over all cases examined. Since these plots
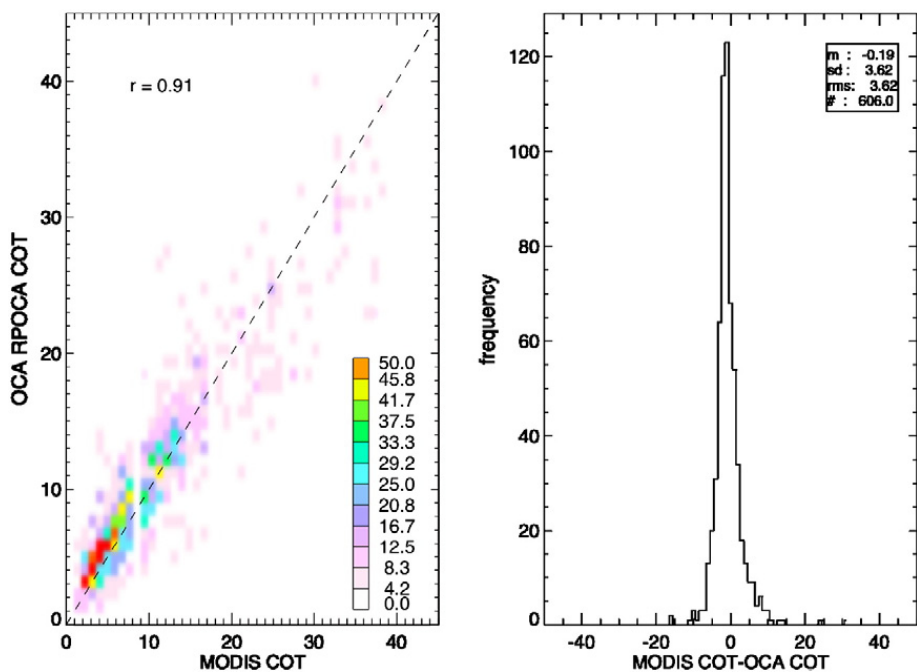

Fig. 4. Comparison of MODIS and OCA cloud optical thickness (unitless; COT or τ) over the Southern Atlantic stratocumulus region from a CPR overpass on 27 August 2006 at 1356 UTC for 593 pixels as shown in Fig. 2b. As in Fig. 3, scatter plot of MODIS to OCA τ comparison (left) and histogram of differences (right). For this plot, the maximum number in a bin is 49. Data are plotted on a linear scale.
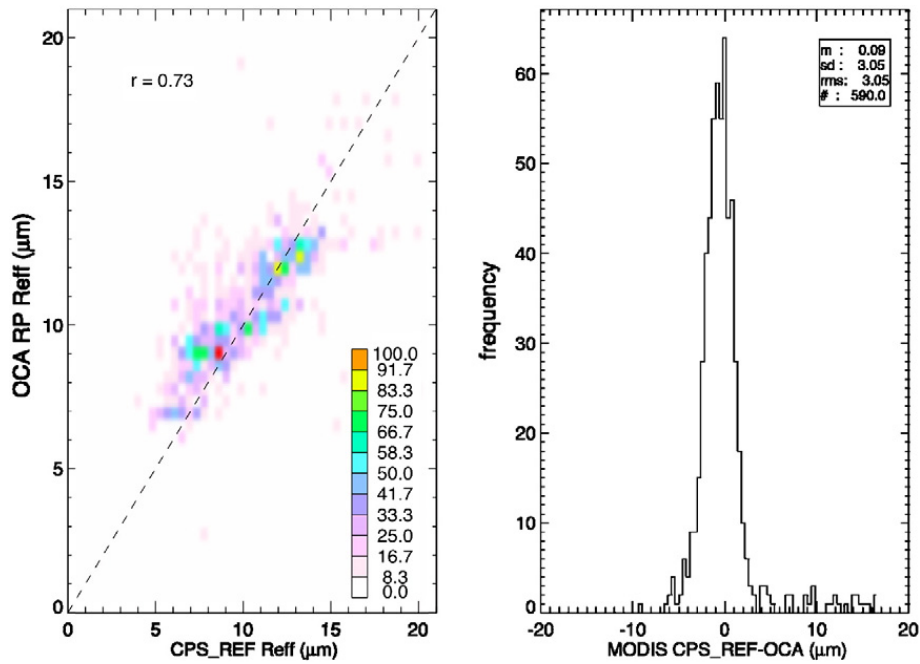
Fig. 5. Comparison of Cloudsat Precipitation Radar (CPS_REF, as in figure) and OCA cloud effective radius (μm; REF, Reff or r_e) over the Southern Atlantic stratocumulus region from a CPR overpass on 27 August 2006 at 1356 UTC for 585 pixels (see Fig. 2b). As in Fig. 4, scatter plot of CPS to OCA r_e comparison (left) and histogram of differences (right). Data are plotted on a linear scale as in Fig. 4. For this plot, the maximum number in a bin is 49. See text for discussion.

represent averages, some of the trends will need explanation toward making a sound interpretation of results. As noted earlier, all data are for the three coldest pixels in the 3×3 box of pixels analyzed per storm.

From Fig. 9(a–h), general patterns are seen. τ (as denoted "COT" in figures) on average generally increases in consistent manners over the 30-min timeframe, with average values increasing on a few days to >100. Some values of τ for individual events reach near 200, which is consistent with

deep convective clouds. We suspect that issues related to cloud geometry at the latitude of the COPS field campaign is a reason why there is such a large deviation over the range of hours covered by the storms studied, ~1000–2330 UTC. The more southern locations (central Italy and the eastern Alps) exhibit the lowest τ overall, again suggesting that satellite angle influences the results. A discussion of the errors and caveats associated with this analysis will be provided in Section 5.3.
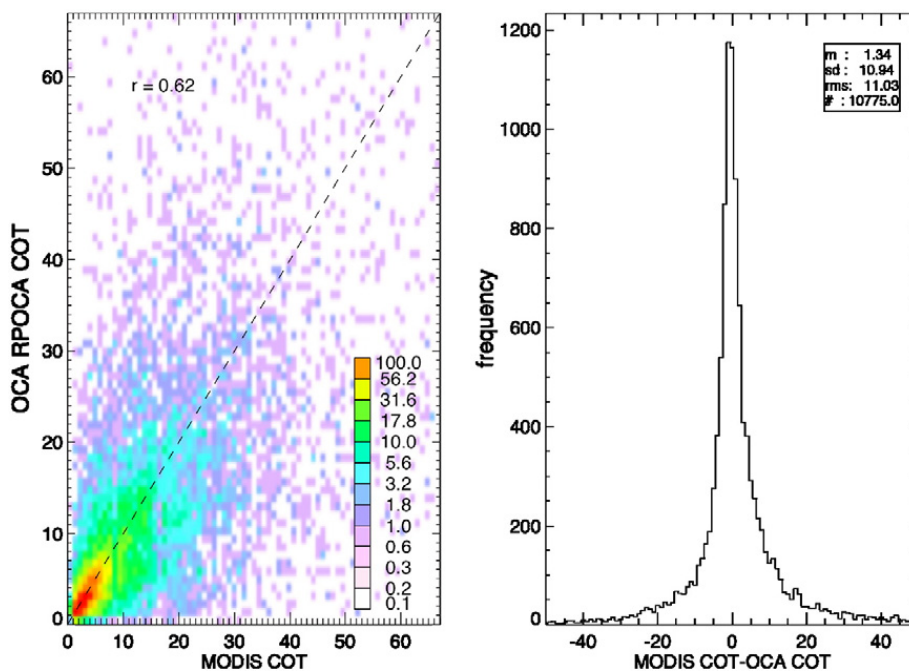

Fig. 6. Log density scatter plot comparison as in Fig. 3, but comparing MODIS and OCA cloud optical thickness (unitless; COT or τ) over all 12 overpasses (Fig. 2a; 11118 pixels) during August 2006 and June 2008, OCA data quality controlled. For this plot, the maximum number in a bin is 164. See text for discussion.
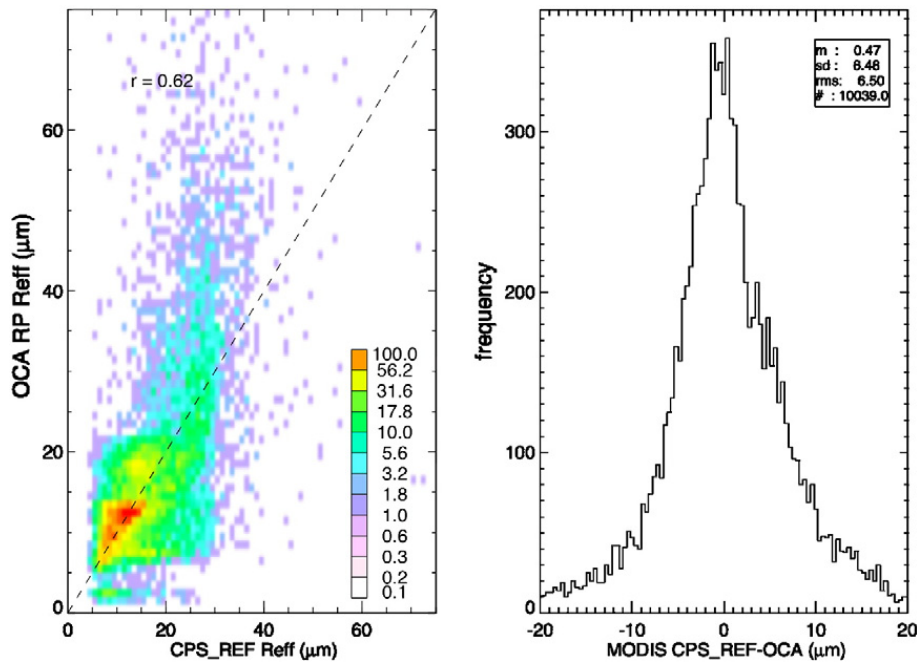
Fig. 7. Log density scatter plot comparison as in Figs. 3 and 6, but comparing of Cloudsat Precipitation Radar (CPS_REF, as in figure) and OCA cloud effective radius (μm; REF, Reff or r_e) over all 12 overpasses (Fig. 2a; 10 037 pixels) during August 2006 and June 2008, OCA data quality controlled. For this plot, the maximum number in a bin is 119. See text for discussion.

With good consistency, p_c values decrease as clouds deepen within a given population of events. Average p_c decreased from 50 to 60 kPa, to between ~33 and 50 kPa over all storms per day or region. The r_e values (denoted as "Re") increase consistently with the τ increase, yet often reach their peak values at times −10 to −5 min, maximizing at ~40–60 μm, before decreasing by 10–20%. We speculate that the r_e decrease is caused by particle settling as the convective clouds deepen.

The J_m exhibits interesting behavior (seen more in the individual cases, Fig. 10), which is related to the OCA retrieval method. J_m values are ≤40 for at least half the 30-min period, with 10–15-min spikes to as high as ~2200 (Fig. 9a). Often, this spike is followed by a decrease in J_m (Fig. 9a–b and g), whereas the basic trend is often upward towards 0 min (Fig. 9d–f and h). From an understanding on how the OCA behaves, these spikes in J_m signify the glaciation process, or more specifically the large misfits within the OCA algorithm when retrieving quantities
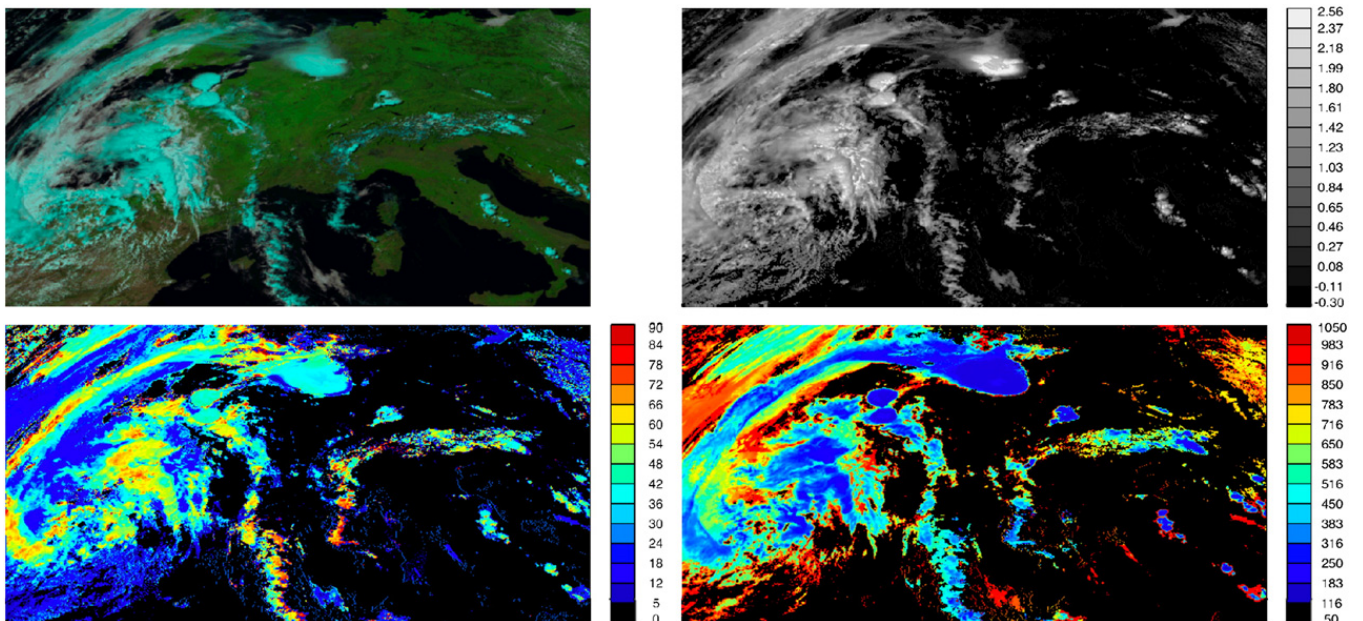

Fig. 8. Clockwise from top-right, an example of a regional plot of a true color image (red the 1.6 μm channel on SEVIRI, green 0.8 μm, and blue 0.6 μm), Log10 cloud optical thickness (τ), r_e (μm), and cloud top pressure (p_c; hPa). All data are for 1320 UTC 25 May 2009, with all parameters plotted without quality control applied except to omit cases with Log10 τ < −0.3 (τ<0.5).
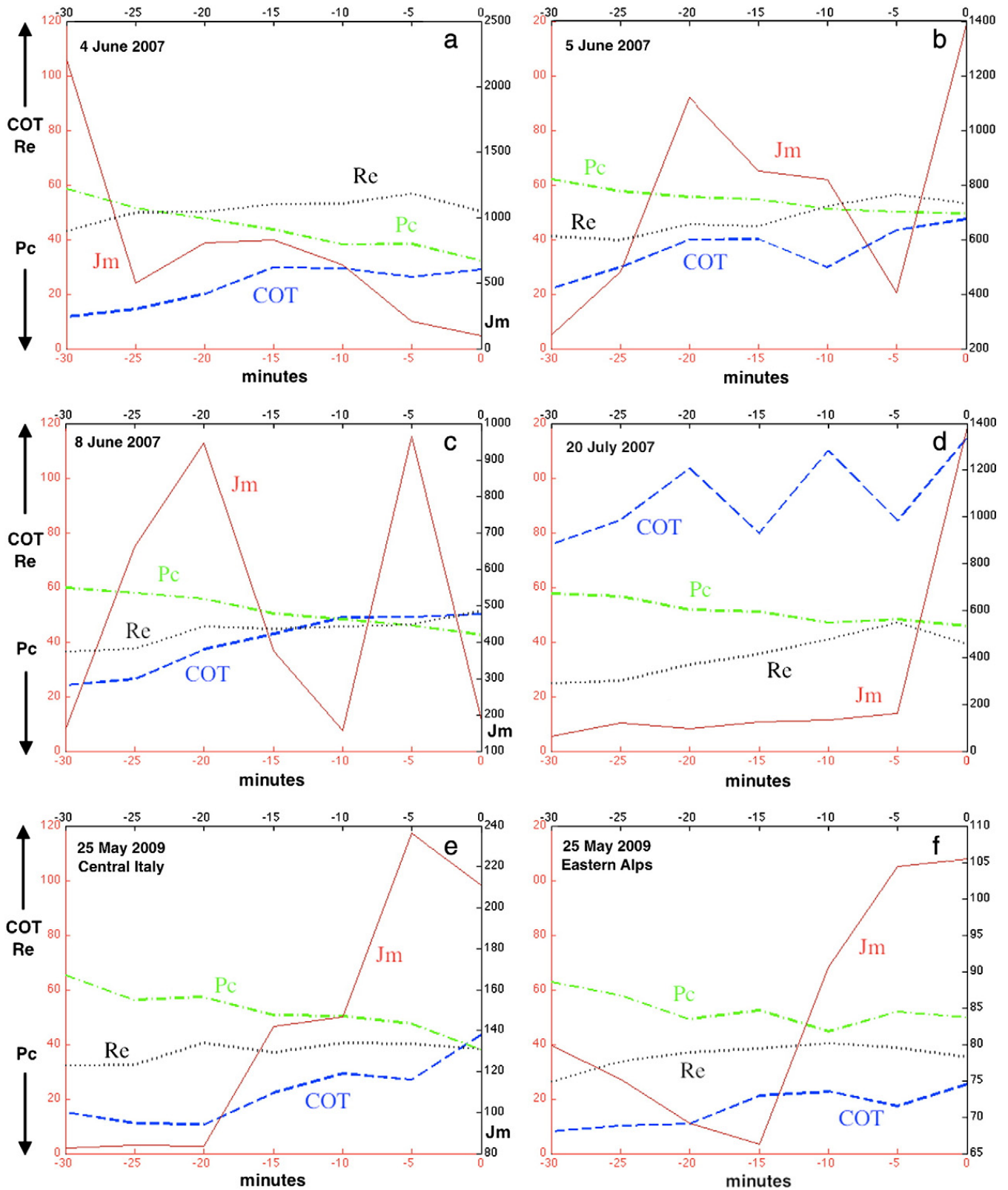
Fig. 9. Per-day or per-region averages of OCA quantities cloud optical depth (COT, or τ as in paper text), cloud-top pressure (Pc), particle effective radius (r_e) and function cost (J_m). Time in minutes is along the abscissa, ranging from -30 to 0 min as various clouds analyzed attained peak COT at various points within this 30-min timeframe. Here, 0 minutes is ~15–45 min in advance of CI, for these events studied. The ordinate is scaled 0–100 [0–120 in (d)], with pressure (kPa) decreasing downward, and J_m (plotted as $J_m \div 10$), COT (unitless) and r_e (μm) increasing upward. Note that not all clouds were progressing through the exact same stage of development, and hence these averages tend to blur the patterns as seen. See text for analysis and additional discussion.
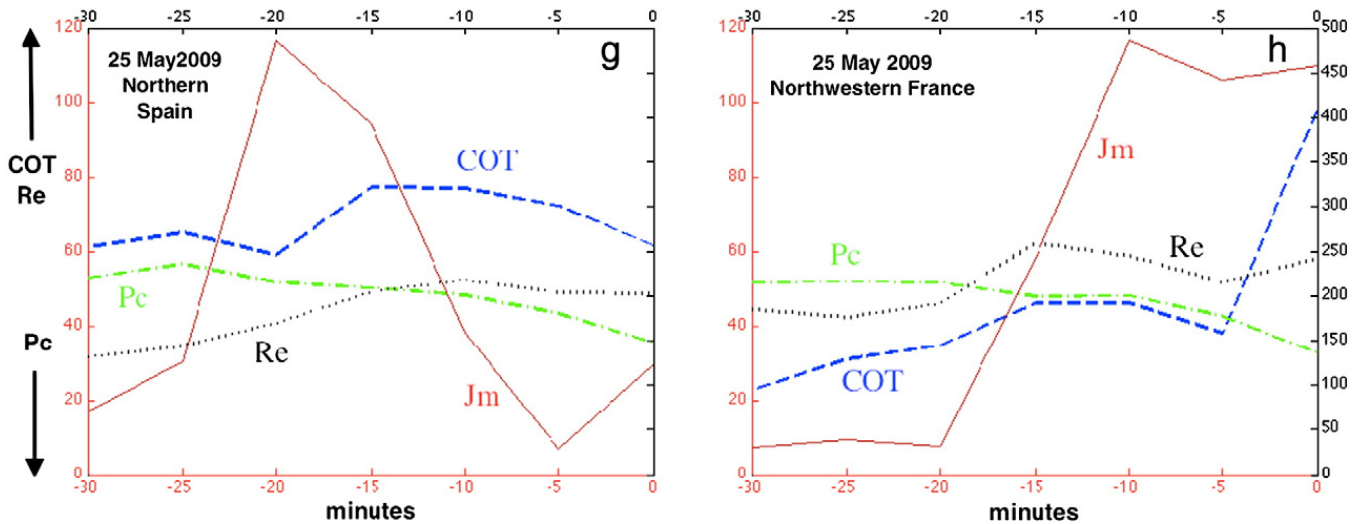
Fig. 9 (continued).

within mixed phase clouds. Lesser misfit ($J_m < 20$) occurs when clouds are either more fully composed of liquid or mostly ice hydrometeors at cloud top. In this way, J_m becomes a non-physical indicator of the phase change. Since the variability in the behavior of J_m is so large in time, the interpretation is that the cumulus clouds studies are in various states of the phase change over the 30-min period, making storm-to-storm comparisons an issue of normalization or percentage changes in J_m with respect to cloud-top glaciation.

Interactions between the four variables include: (a) a tendency for J_m to peak at or before the maximum τ is attained, by up ~5–10 min, (b) the largest retrieved r_e occur nearly at the time of τ maximum, and (c) maximum r_e values are found to occur within 5–10 min before J_m reaches its peak value. The interpretation is that r_e increases during the time of phase change, and decreases thereafter once ice particles dominate and begin settling downward. Yet, there appears to be little relationship in time between the largest J_m and the largest r_e values, suggesting that particle sizes vary substantially from storm to storm in advance of CI, and that averaging may be blurring the results (see discussion for individual storms below). Overall, the tendency of τ peaking, or beginning to trend downward, suggests a convective cloud of relative deep vertical extent with a glaciated top.

5.2. Per-storm and composite analyses

Four individual, representative events from the 94-cloud population are shown in Fig. 10(a–d), in a similar fashion to Fig. 9(a–h). For these events, spread over a 30-min time window, not all clouds were necessarily progressing through the same stage of development, and therefore, the discussion will focus on relationships between fields rather than how fields relate to specific times.

For all events, the following features are found: (1) τ values increase over time, exhibiting a positive time rate of change, often with a sudden jump in magnitude over 5–10-min periods, (2) p_c values decrease as clouds deepen, beginning near 80 kPa in Fig. 10(a–b), (3) r_e values show two trend types: to generally increase then decrease (Fig. 10b and c), or a slow decrease (Fig. 10a and d), and (4) like in

Fig. 9(a–h), J_m values tend to show a distinct maxima which precede or are coincident with a general increase in τ values (except in Fig. 10a). We interpret these behaviors as the phase change occurring near the increase or spike in J_m (as in Fig. 9), with cloud deepening denoted by the rapid increase in τ, to >250 in Fig. 10d. Recall from before, the peak in J_m signifies the OCA algorithm's inability to fit a solution to either a pure water or a pure ice model for hydrometeors, and represents a non-physical way of identifying the clouds deepening and glaciating.

Also plotted in Fig. 10(a–d) are 10.8 μm T_B values for the coldest pixel in the 3×3 analysis box for the cumulus clouds examined. These temperatures mimic the p_c trends well, decreasing by 10 to >35 K over the 30-min period. One issue likely confounding these results are slight changes in the cumulus cloud target over the analysis time, specifically, what is the character of the cumulus clouds within respect to a target box (the three coldest 10.8 μm pixels) from time to time, which is apparent in Fig. 10b (the wavering behavior in T_B between −10 and 0 min). Specifically, the cloud tops may warm and cool slightly as clouds do not filling an entire pixel, or as a cloud becomes span by adjoining IR pixels. We consider these artifacts unavoidable as clouds evolve, and as circular cloud features are being observed by SEVIRI pixels (in contrast to fitting surfaces to the cloud parameters).

Fig. 11(a–b) shows r_e as a function of p_c [or temperature as a function of pressure, $T(p)$ as in Fig. 11a] for a cluster of growing convective clouds on 4 June 2007 (Fig. 10a), and for all 94 events over the 0–30-min period (Fig. 11b). This is shown to demonstrate the variability in r_e as a function of time and cloud depth, as retrieved from the OCA model. General patterns include a tendency for a decrease in r_e (from ~38 to 25 μm) for cloud tops generally warmer than −10 °C or below ~600 hPa, an increase in r_e (from ~25 to 70–80 μm) as clouds cool to the homogeneous freezing point (−38 to −40 °C, or ~350 hPa; Rosenfeld and Woodley, 2000), followed by a gradual decrease in r_e as cloud tops cool to −60 °C or extend above 250 hPa. These patterns describe the following processes: first, the presence of small particles at cloud top as new clouds grow vertically while hydrometeors are mainly liquid (mostly below ~600 hPa); second, the process of particle
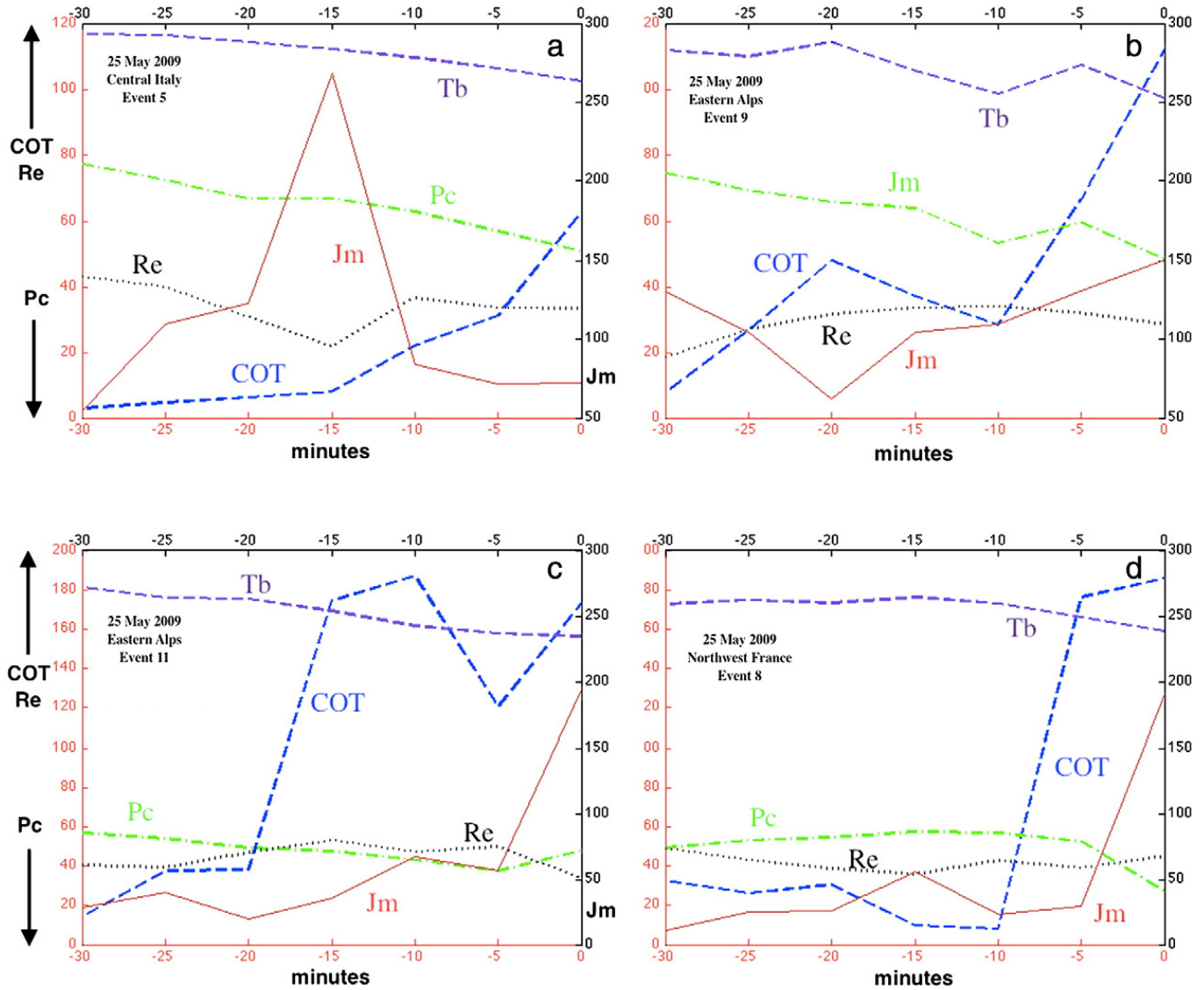
Fig. 10. Same as Fig. 9(a–h), yet for individual growing cumulus cloud events within the 94–storm database (see Table 1). Also plotted here is the 10.8 μm brightness temperature for the single coldest pixel in the 3 × 3 analysis box as described in Section 3 ("Tb" in figure; the right-hand scale applies to both Jm and Tb). See text for analysis and discussion.

sizes increasing rapidly in the mixed phase portion of the cloud (−10 to −40 °C); and third, the trend of decreasing particle sizes in high portions of cumuli as a result of gravitational settling. Also, nearly all r_e values are >14 μm, the threshold determined for cloud droplets to initiate the precipitation process in optically thick clouds ($\tau \geq \sim 9$; Rosenfeld and Gutman, 1994), as is the case for the cumuli being studied.

Returning to Fig. 9, and especially Fig. 10(a–b) which includes cloud-top T_B, in comparison to Fig. 11(a–b), the following results are highlighted: First, there is a general trend of r_e increasing, followed by a leveling off or decrease in r_e values, suggests that cloud-top temperatures within the 94 storm database are between 0 and −30 °C. For growing cumulus on the colder side of this range, we suspect that >35-dBZ intensity rainfall may already have been occurring by the 0-min point, or was present aloft, and reached the ground within 15 min. Second, from Fig. 10 (a–b) it is found that for the periods of r_e increase (−15 to −10 min in Fig. 10a; −30 to −10 min in Fig. 10b; −25 to −15 min in Fig. 10c; and −15 to 0 min in Fig. 10d), T_B values are within the +10° to −25 °C range. Specifically, r_e growth is found

from 0 to −10 °C (Fig. 10a), +10° to −10 °C (Fig. 10b), 0° to −20 °C (Fig. 10c), and −10° to −25 °C (Fig. 10d), which is consistent with the patterns seen in Fig. 11(a–b) for particle growth between ~0° and −38 °C. The exception is growth at temperatures above 0 °C as seen in Fig. 10b (between −30 and −20 min).

As a means of showing the overall statistics of the events studied, Fig. 12(a–d) shows box (also known as "box and whiskers") plots for the four OCA variables. These plots corroborate the analysis presented in Figs. 9 and 10. Each box-plot has a notched box representing the middle 50% of the data, or inter-quartile range (IQR). A larger IQR (notch size) indicates higher data spread or variability. The horizontal black line splitting the box into two equal segments is the median (Wilks, 2006, pp. 26–31). The vertical dashed lines on either side of the IQR (the whiskers) represent ~99% of the distribution, from whisker to whisker. Circles beyond the whiskers signify outlier data points. As a visual statistical significance test, notch-overlap verifies whether each dataset (for a given time) is significantly different than another, and
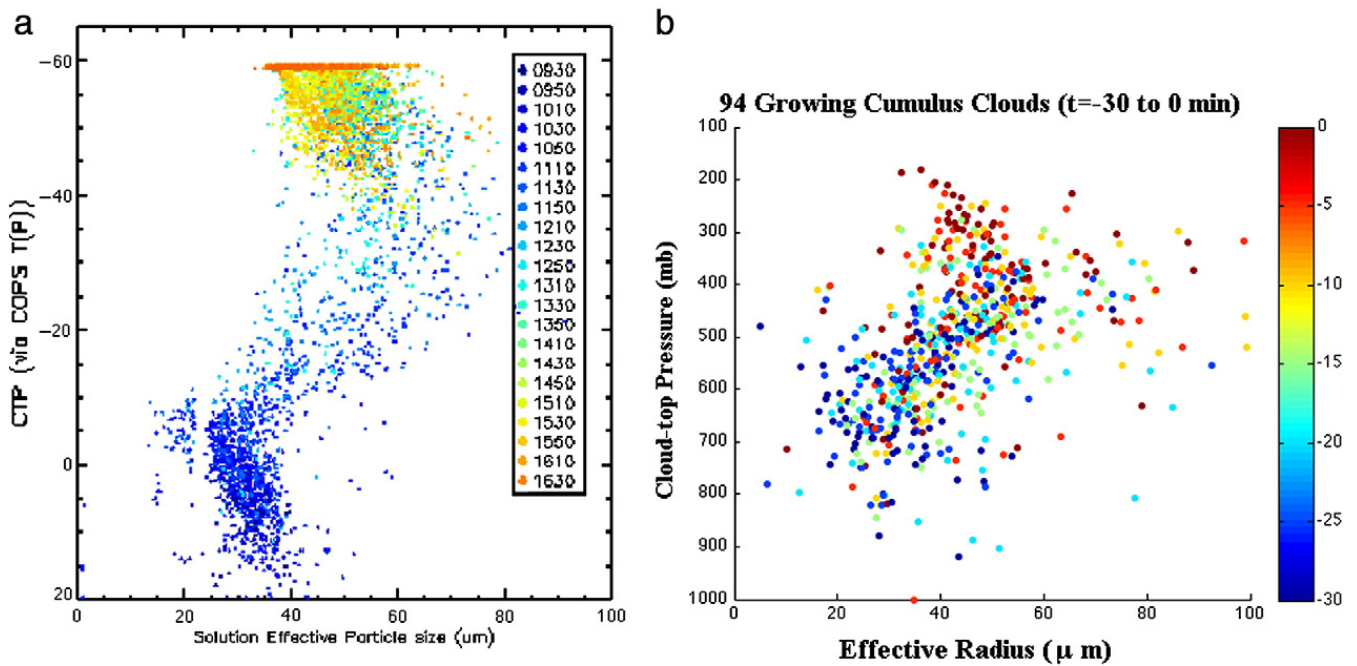
Fig. 11. (a) Particle effective radius (r_e; μm) versus cloud top pressure (CTP) [converted to temperature, T(p)], over an analysis from 0930–1630 UTC for a cluster of convective storms on 4 June 2007 during the COPS field campaign, for only cumulus cloud pixels. All data plotted are for $J_m \geq 200$. (b) r_e versus cloud top pressure (c_p; millibars) for all 5-min periods in the 94-event database. In Fig. 11a, dots are colored according to time, 0930 to 1630 UTC (and hence the depth of the cumulus cloud). In Fig. 11b, dots are also colored according to time within the 30–min analysis window for all 94 events analyzed. Fig. 11a exemplifies changes in r_e over a cluster of convective clouds as they grow from cumulus to *cumulonimbus*, while Fig. 11b illustrates the r_e changes only over the 30-min time as cumulus clouds deepen.

when two per-time datasets are deemed statistically the same at the 0.05-level. The 5% test level (a common threshold) allows one to accept that the notch-overlap hypothesis test is correctly assessing the results ≥95% of the time. Notches that do not overlap indicate that the two datasets are significantly different.

In Fig. 12a, τ values increase to −10 min, and then are more variable (implying a steady trend from −10 to 0 min, or highly variable τ values between events). The variability, denoted by the notch size, is largest at the final time, as is the overall spread in the data. The J_m data (Fig. 12b) (without being divided by 10 as above) show the same maxima midway through the period, with the largest J_m seen at −10 and 0 min. The largest variability is after −15 min, and together with the previous observation, show that the glaciation process (when the OCA algorithm exhibits large uncertainty) occurs on average after −15 min in the events analyzed.

Fig. 12c shows well-behaved p_c statistics, describing cumulus cloud growth. Fig. 12d shows how r_e values increase to approximately the −15 min time, before leveling off, for reasons related to particle settling as described above, leading to decreasing r_e values at cloud top toward 0–min (which is only slightly apparent as the distributions spread decreases at the −5 to 0 min times).

5.3. Issues of variability and error in OCA retrievals

In much of the foregoing analysis cloud-to-cloud variability is substantial, whereas averaging of several storms together (e.g., daily or regional averages) leads to smoother results. Reasons for the large variability are discussed here as a means of describing limitations of the OCA (or any current procedure, for

that matter) when describing cloud-top microphysical properties in 3 km sampling distance IR data.

Perhaps one of the weaknesses of using solar reflectance channel information (via the 0.6, 0.8 and 1.6 μm channels) when analyzing growing convective clouds using the OCA is the dependence on geometry. Small and medium growing cumulus are highly structured objects and, depending on the location of a pixel to the cloud's core, the effective solar-satellite geometry of the reflecting cloud surface can be significantly different to that given by an assumed horizontal surface. With high solar angles (near solar noon) the effects are minimal, however, early and late developing clouds are subject to distinctly uneven illumination. Given that clouds were analyzed over a range of times per day we expect that cloud geometry issues will increase the variability (noise) in the results.

While there is evidence that the quality control offered by the OCA J_m mitigates the cloud geometry problem, it is clear that many non-horizontal scenes give J_m lower than the thresholds used here. The consequences of such illumination problems are erroneously high (low) τ retrievals on illuminated (shaded) cloud sides. Consequences for r_e retrievals are in principle less obvious because of the dependence on τ in the interpretation, but for thick clouds the r_e would be expected to be low (high) for illuminated (shaded) targets.

We expect the IR channel's sensitivity to geometry (as used in OCA) to be significantly less; emissivity varies with emission angle but strong effects are only found at angles >60°, and with the COPS area view angles around 50° very strong average cloud slopes would be required to give a noticeable effect. Also, because this analysis was subjective, performed by a human expert, we expect that errors caused by cloud tracking to be minimal. Errors caused by convective clouds not filling an entire 3 km MSG pixel will lead to a substantial problems with any
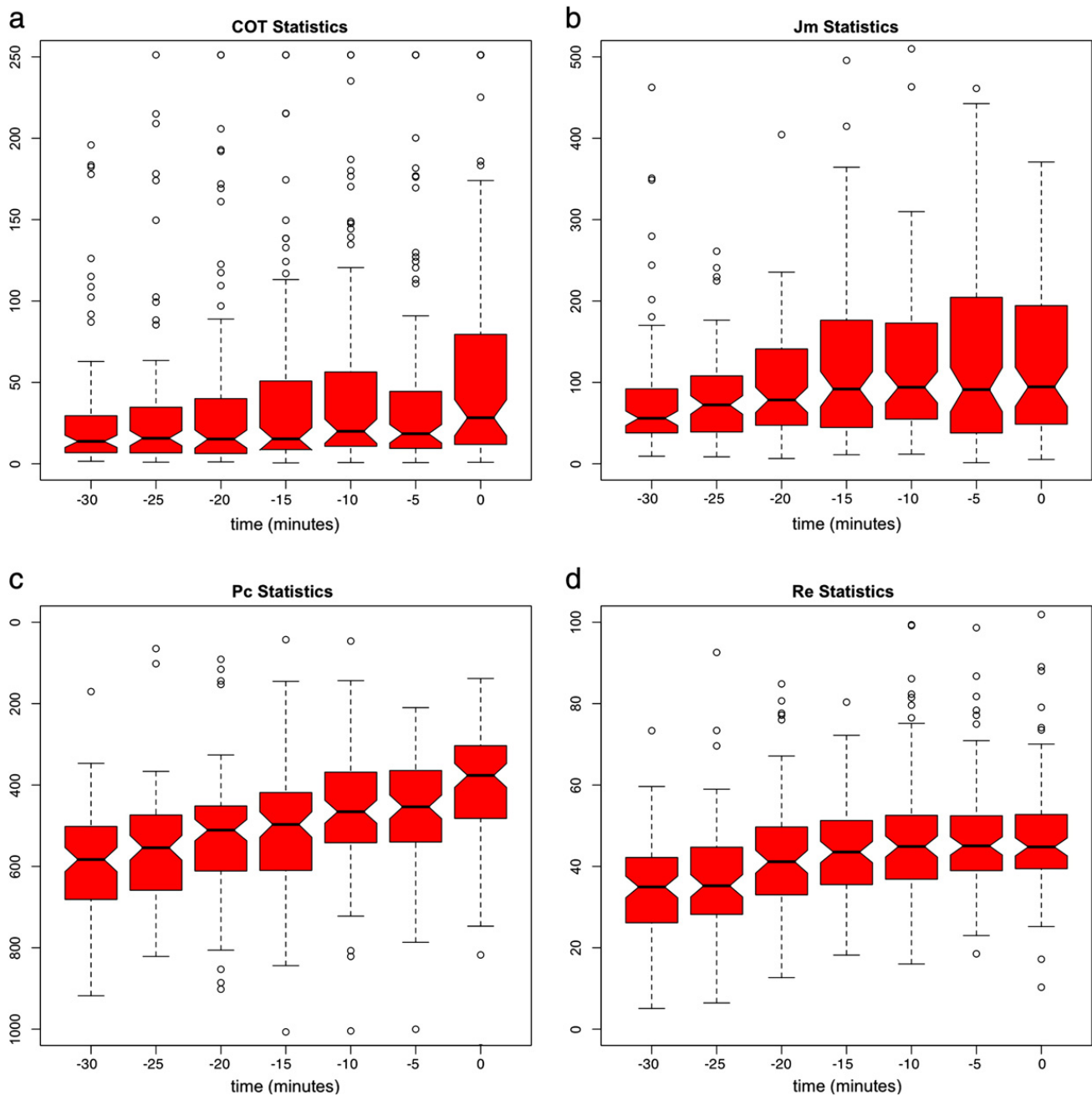
Fig. 12. Statistical representation (in the form of box, or "box and whiskers" plots) of cloud optical depth (COT, unitless), cloud-top pressure (Pc, hPa), particle effective radius (Re, μm) and function cost (Jm, unitless) for all 94 events. Attributes of plots are described in the text.

retrieval algorithm like OCA, such that sub-pixel contributions from the surface will certainly lead to artificially warm cloud temperatures. As the OCA fields used in this study does not rely on the 3.9 μm channel, and because the clouds being examined are "optically thick," sub–pixel responses from Earth's surface will not result in spurious retrieval results (Watts et al., 1998; Poulsen et al., 2011).

6. Discussion and conclusions

The above study has demonstrated how several cloud–top properties can be interpreted for growing convective clouds, when analyzed at 5-min intervals before the clouds are mature and producing rainfall at the ground. The main goals of the study were to understand how OCA retrieved fields, τ, r_e, p_c and J_m, for growing convective clouds, at 5-min temporal resolution, may be used to understand cloud top and in-cloud processes associated with cumulus cloud growth. These include updraft strength and phase changes related to r_e changes, τ as a function of cloud depth, and cloud longevity. Identifying these interactions will help extend our understanding of cloud-top–in-cloud relationships, to promote the use of OCA-like products for convective cloud diagnosis, and to incorporate retrieved microphysical fields within algorithms that nowcast (0–1-h forecast) new thunderstorm formation or intensity.

The validity of the OCA data is presented with a comparison to MODIS and CPR retrieved cloud properties. Subsequently,

results from the analysis of OCA fields for all events show that as cumuli deepen, r_e values increase, and then decrease in size as cloud tops glaciate and particle settling begins. The τ magnitudes generally increase as clouds deepen, while p_c falls as expected. The J_m values exhibit the interesting pattern of a defined spike within the 30-min period, which indicates the increase misfit within OCA during the mixed phase, at the time r_e values begin increasing as larger ice particles form. Lastly, discussion on how OCA fields may be used within a real-time system for monitoring convective clouds in advance of thunderstorm development is provided.

The main results with respect to OCA fields are: (1) OCA fields evolve consistently as cumulus clouds deepen, with τ exhibiting a positive time rate of change, p_c decreasing as clouds deepen, r_e values show two trend types: to increase and then decrease, or to remain generally steady, and J_m values show a distinct maxima which precedes an increase in r_e values. (2) The per-storm maximum in J_m maxima are related to the phase change, as a result of increased misfit between either a pure water or pure ice model in the retrieval process. (3) On per-storm bases, τ values increase rapidly over 5–10-min periods, suggesting a period of rapid cloud deepening. (4) As an average, over 94 events, τ and J_m show similarly trends to increase from -30 to -10 min, followed by a substantial (10–20%) decrease, before rising toward 0 min; this is speculated to be related to cloud-top glaciation, while the decrease in τ is less easily explained. And, (5) the distribution spread in τ, J_m and r_e all increase between -15 and -5 min (or basically toward the end of the analysis time period), again suggesting less certainty in the OCA analyses, but also highlighting phase change at cloud top.

From Figs. 9 and 10, no specific rate of change in τ can be associated with changes in r_e or p_c. Yet, for specific cases, rapid increases in τ occur at some point in the 30-min analysis window as in Fig. 10(a–d), while p_c and T_B values fall consistently. We speculate that such consistent relationships exist between τ changes and those in r_e or p_c, but they appear to be unsystematic, and likely are strongly influenced by local environmental factors such as precipitable water (to make in-cloud humidity and ice water path higher), aerosols (e.g., Lindsey et al., 2010), and boundary layer humidity (which determines cloud-base height and updraft humidity).

An analysis of vertical motion as deduced from p_c values (i.e. creating an ω, hPa s^{-1}) showed very low correlation to r_e values ($+0.2$; decreasing r_e for decreasing ω) as a general rule, suggesting that within the population of events analyzed here by OCA, no strong relationships are found similar to those developed in Rosenfeld et al. (2008). The error sources discussed in Section 5.3, specifically related to viewing geometry for ≤ 3 km^2 cumulus clouds, may lead to this relationship being so weak.

The advice from this study is that when using OCA (or OCA-like) fields to analyze convective storm development, relative changes are more important to monitor than absolute changes. Therefore, the simple threshold methods employed to CI interest fields, (for 0–1-h CI nowcasting) in studies by Robert and Rutledge (2003), Mecikalski et al. (2006, 2008, 2010a,b) and Siewert et al. (2010) should be altered by considering the regional behavior of convection. This would imply that there would be benefit in employing

methods such as "time–space exchangeability" (Lensky and Rosenfeld, 2006; Yuan et al., 2008) toward removing the local mean (or mean time tendency), focusing on perturbations of the OCA fields before using them to characterize the growth rates or vigor of convective clouds. In essence, local extremes of r_e, τ or p_c can be used to isolate locally vigorous updrafts.

Therefore, practical methods for including OCA fields into an operational or real-time convective nowcasting system include: (a) evaluating time rates of change for growing cumuli as opposed to absolute magnitudes of OCA fields so to decrease the reliance on specific values per cumulus cloud, (b) focusing on r_e toward quantifying the phase change process, (c) using τ data to monitor the rapid thickening of cumulus towers, (d) especially as sensor resolutions increase to >3 km on forthcoming geostationary sensors (e.g., Meteosat Third Generation, GOES–R), using r_e fields in a relative sense to indeed quantify which convective cloud possess locally strong updrafts, for gauging storm intensity, and (e) testing the 3.9 μm (in place of 1.6 μm) data for use during nighttime settings.

Follow-on work will include using OCA fields to potentially solve outstanding problems in CI nowcasting related to the detection of convective cloud growth beneath thin cirrus. Presently, CI often goes undetected when cumulus clouds are obscured by higher-level cirrus clouds, whereas an increase in τ would imply local cloud development, especially if the horizontal scales were ~8 km or less. The main benefit of OCA data in analyzing growing cumuli prior to CI is the advanced indication they provide of the glaciation process, which is key to precipitation formation when ice processes are involved. In "warm–topped" convection (when ice is absent, or unimportant), increases in τ and r_e would signify the development of precipitation within a deepening cloud. Additionally then, J_m values remaining low as cumulus clouds continue to deepen (as τ values rise) would be an important delineator of "warm rain" microphysics (e.g., Chien and Neiburger, 1972), and therefore would be valuable in nowcasting CI in tropical and oceanic convective regimes, a substantial advantage over current CI nowcasting methods.

Ongoing research is toward implementing the finding of this study in current CI and convective storm nowcasting systems, towards increasing their detection accuracy, and abilities to monitor convective behavior and mode over a storm's life cycle. Such systems include Corridor Integrated Weather System (CIWS; Dupree et al., 2005; Wolfson and Clark, 2006)], the Thunderstorm Identification, Tracking, and Nowcasting (TITAN; Han et al., 2009), Cb-TRAM (Zinner et al., 2008), and the Autonowcaster (Mueller et al., 2003).

Acknowledgements

References

Arking, A., Childs, J.D., 1985. Retrieval of cloud cover parameters from multi-spectral satellite images. J. Climate Appl. Meteorol. 24, 322–333.

Baum, B.A., Spinhirne, J.D., 2000. Remote sensing of cloud properties using MODIS airborne simulator imagery during SUCCESS. 3. Cloud overlap. J. Geophys. Res. 105 (D9), 11793–11804.

Baum, B.A., Wielicki, B.A., Minnis, P., Parker, L., 1992. Cloud-property retrieval using merged HIRS and AVHRR data. J. Appl. Meteorol. 31, 351–369.

Baum, B.A., Kratz, D.P., Yang, P., Ou, S., Hu, Y., Soulen, P.F., Tsay, S.-C., 2000a. Remote sensing of cloud properties using MODIS airborne simulator imagery during SUCCESS. 1. Data and models. J. Geophys. Res. 105 (D9), 11767–11780.

Baum, B.A., Soulen, P.F., Strabala, K.I., King, M.D., Ackerman, S.A., Menzel, W.P., Yang, P., 2000b. Remote sensing of cloud properties using MODIS airborne simulator imagery during SUCCESS. 2. Cloud thermodynamic phase. J. Geophys. Res. 105 (D5), 11781–11792.

Chin, E.H.C., Neiburger, M., 1972. A numerical sumulation of the gravitational coagulation process for cloud droplets. J. Atmos. Sci. 29, 718–727.

Dong, X., Minnis, P., Mace, G.G., Smith Jr., W.L., Poellot, M., Marchand, R.T., Rapp, A.D., 2002. Comparison of stratus cloud properties deduced from surface, GOES, and aircraft data during the March 2000 ARM Cloud IOP. J. Atmos. Sci. 59, 3256–3284.

Dong, X., Minnis, P., Xi, B., 2005. A climatology of midlatitude continental clouds from the ARM SGP Central Facility: Part I: Low-level cloud macrophysical, microphysical and radiative properties. J. Climate 18, 1391–1410.

Dong, X., Xi, B., Minnis, P., 2006. A climatology of midlatitude continental clouds from the ARM SGP Central Facility: Part II: Cloud fraction and radiative forcing. J. Climate 19, 1765–1783.

Dong, X., Minnis, P., Xi, B., Sun-Mack, S., Chen, Y., 2008. Comparison of CERES-MODIS stratus cloud properties with ground-based measurements at the DOE ARM Southern Great Plains site. J. Geophys. Res. 113, D03204. doi:10.1029/2007JD008438.

Duda, D.P., Minnis, P., Nguyen, L., 2001. Estimates of cloud radiative forcing in contrail clusters using GOES imagery. J. Geophys. Res. 106, 4927–4937.

Duda, D.P., Minnis, P., Palikonda, R., 2004. A case study of the development of contrail clusters over the Great Lakes. J. Atmos. Sci. 1132–1146.

Dupree, W.J., Wolfson, M.M., Johnson Jr., R.J., Boldi, R.A., Mann, E.B., Theriault Calden, K., Wilson, C.A., Bieringer, P.E., Martin, B.D., Iskenderian, H., 2005. FAA tactical weather forecasting in the United States national airspace. World Weather Research Program, Symposium on Nowcasting and Very Short Range Forecasting, Toulouse, France.

EUMETSAT, 2007a. MSG Level 1.5 Image Data Format Description, Publication EUM/MSG/ICD/105. 122 pp. [Available from EUMETSAT, Am Kavalleriesand 31, D-64295 Darmstadt, Germany.].

EUMETSAT, 2007b. Cloud Detection for Meteosat Second Generation—Algorithm Theoretical Basis Document, EUM/MET/REP/07/0132, EUMETSAT, EUMETSAT Alle 1, D-64295. Darmstadt, Germany.

Fan, J., Yuan, T., Comstock, J.M., Ghan, S., Khain, A., Leung, L.R., Li, Z., Martins, V.J., Ovchinnikov, M., 2009. Dominant role by vertical wind shear in regulating aerosol effects on deep convective clouds. J. Geophys. Res. 114, D22206. doi:10.1029/2009JD012352.

Greenwald, T.J., Christopher, S.A., 2000. The GOES I–M Imagers: new tools for studying microphysical properties of boundary layer stratiform clouds. Bull. Am. Meteorol. Soc. 81, 260–2619.

Han, L., Fu, S., Zhao, L., Zheng, Y., Wang, H., Lin, Y., 2009. 3D convective storm identification, tracking, and forecasting—an enhanced TITAN algorithm. J. Atmos. Oceanic Technol. 26, 719–732.

Heidinger, A.K., Pavolonis, M.J., 2009. Gazing at cirrus clouds for 25 years through a split window, part 1: methodology. J. Appl. Meteorol. Climatol. 48, 1100–1116.

Hulley, G.C., Hook, S.J., 2008. A new methodology for cloud detection and classification with ASTER data. Geophys. Res. Lett. 35, L16812. doi:10.1029/ 2008GL034644.

Hutchison, K.D., Etherton, P.J., Topping, P.C., Huang, H.L., 1997. Cloud top phase determination from the fusion of signatures in daytime AVHRR imagery and HIRS data. Int. J. Remote Sens. 18, 3245–3262.

Kidder, S.Q., Vonder Haar, T.H., 1995. Satellite Meteorology. Academic Press, San Diego, CA. 466 pp.

King, M.D., Tsay, S.-C., Platnick, S.E., Wang, M., Liou, K.-N., 1998. Cloud retrieval algorithms for MODIS: optical thickness, effective particle radius, and thermodynamic phase. MODIS Algorithm Theoretical Basis Document No. ATBD-MOD-05 (version 5, December 1997). 79 pp.

Lensky, I.M., Rosenfeld, D., 2006. Clouds-aerosols-precipitation satellite analysis tool (CAPSAT). Atmos. Chem. Phys. 8, 6739–6753.

Lindsey, D.T., Grasso, L.D., 2008. An effective radius retrieval for thick ice clouds using GOES. J. Appl. Meteorol. Climatol. 47, 1222–1231.

Lindsey, D.T., Hillger, D.W., Grasso, L., Knaff, J.A., Dostalek, J.F., 2006. GOES climatology and analysis of thunderstorms with enhanced 3.9-μm reflectivity. Mon. Weather Rev. 134, 2342–2353.

Lindsey, D.T., Miller, S.D., Grasso, L., 2010. The impacts of the 9 April 2009 dust and smoke on convection. Bull. Am. Meteorol. Soc. 91, 991–995.

Liou, K.N., 1992. Radiation and cloud processes in the atmosphere. Oxford Monographs on Geology and Geophysics No. 20. Oxford University Press, Inc, New York, NY. 487 pp.

Lopez, M.A., Hartmann, D.L., Blossey, P.N., Wood, R., Bretherton, C.S., Kubar, T.L., 2009. A test of the simulation of tropical convective cloudiness by a cloud-resolving model. J. Climate 22, 2834–2849.

Mecikalski, J.R., Bedka, K.M., 2006. Forecasting convective initiation by monitoring the evolution of moving cumulus in daytime GOES imagery. Mon. Weather Rev. 134, 49–78.

Mecikalski, J.R., Paech, S.J., Bedka, K.M., Litten, L.A., 2008. A statistical evaluation of GOES cloud-top properties for nowcasting convective initiation. Mon. Weather Rev. 136, 4899–4914.

Mecikalski, J.R., Mackenzie, W.M., Koenig, M., Muller, S., 2010a. Use of Meteosat Second Generation infrared data in 0–1 hour convective initiation nowcasting. Part 1. Infrared fields. J. Appl. Meteorol. Climate 49, 521–534.

Mecikalski, J.R., Mackenzie, W.M., Koenig, M., Muller, S., 2010b. Use of Meteosat Second Generation infrared data in 0–1 hour convective initiation nowcasting. Part 2. Use of visible reflectance. J. Appl. Meteorol. Climate 49, 2544–2558.

Menzel, W.P., Frey, R.A., Baum, B.A., 2010. Cloud top properties and cloud phase — MODIS algorithm theoretical basis document. (version 8, October 2010), 62 pp.

Min, Q., Harrison, L.C., 1996. Cloud properties derived from surface MFRSR measurements and comparisons with GOES results of the ARM SETP site. Geophys. Res. Lett. 23, 2784–2786.

Minnis, P., Garber, D.P., Young, D.F., Arduini, R.F., Takano, Y., 1998. Parameterization of reflectance and effective emittance for satellite remote sensing of cloud properties. J. Atmos. Sci. 55, 3313–3339.

Minnis, P., Schumann, U., Doelling, D.R., Gierens, K.M., Fahey, D.W., 1999. Global distribution of contrail radiative forcing. Geophys. Res. Lett. 26. doi:10.1029/ 1999GL900358.

Minnis, P., Smith Jr., W.L., Nguyen, L., Khaiyer, M.M., Spangenberg, D.A., Heck, P.W., Palikonda, R., Bernstein, B.C., McDonough, F., 2004a. A real-time satellite-based icing detection system. Proc. 14th Intl. Conf. Clouds and Precipitation, Bologna, Italy, 18–23 July.

Minnis, P., Gambheer, A.V., Doelling, D.R., 2004b. Azimuthal anisotropy of longwave and infrared window radiances from the clouds and the earth's radiant energy system on the Tropical Rainfall Measuring Mission and Terra satellites. J. Geophys. Res. 109, D08202. doi:10.1029/2003JD004471.

Minnis, P., Yost, C.R., Sun-Mack, S., Chen, Y., 2008. Estimating the top altitude of optically thick ice clouds from thermal infrared satellite observations using CALIPSO data. Geophys. Res. Lett. 35, L12801. doi:10.1029/ 2008GL033947.

Mueller, C., Saxen, T., Roberts, R., Wilson, J., Betancourt, T., Dettling, S., Oien, N., Yee, J., 2003. NCAR Auto-Nowcast system. Weather Forecast. 18, 545–561.

Nakajima, T., King, M.D., 1990. Determination of the optical thickness and effective particle radius of clouds from reflected solar radiation measurements. Part 1: Theory. J. Atmos. Sci. 47, 1878–1893.

Nakajima, T.Y., Nakajima, T., 1995. Wide area determination of cloud microphysical properties from NOAA AVHRR measurements for FIRE and ASTEX. J. Atmos. Sci. 52, 4043–4059.

Parol, F., Buriez, J.-C., Brogniez, G., Fourquart, Y., 1991. Information content of AVHRR channels 4 and 5 with respect to the effective radius of cirrus cloud properties. J. Appl. Meteorol. 30, 973–984.

Pavolonis, M.J., Heidinger, A.K., 2004. Daytime cloud overlap detection from AVHRR and VIIRS. J. Appl. Meteorol. 43, 762–778.

Pavolonis, M.J., Heidinger, A.K., Uttal, T., 2005. Daytime global cloud typing from AVHRR and VIIRS: Algorithm description, validation, and comparisons. J. Appl. Meteorol. 44, 804–826.

Poulsen, C.A., Watts, P.D., Thomas, G.E., Sayer, A.M., Siddans, R., Grainger, R.G., Lawrence, B.N., Campmany, E., Dean, S.M., Arnold, C., 2011. Cloud retrievals from satellite data using optimal estimation: Evaluation and application to ATSR. Atmos. Meas. Tech. Discuss. 4, 2389–2431. doi:10.5194/amtd-4-2389-2011.

Roberts, R.D., Rutledge, S., 2003. Nowcasting storm initiation and growth using GOES–8 and WSR–88D data. Weather Forecast. 18, 562–584.

Rosenfeld, D., Gutman, G., 1994. Retrieving microphysical properties near the tops of potential rain clouds by multispectral analysis of AVHRR data. Atmos. Res. 34 (1–4), 259–283.

Rosenfeld, D., Woodley, W.L., 2000. Deep convective clouds with sustained supercooled water down to − 37.5 °C. Nature 405, 440–441 (May 2000).

Rosenfeld, D., Woodley, W.L., Lerner, A., Kelman, G., Lindsey, D.T., 2008. Satellite detection of severe convective storms by their retrieved vertical profiles of cloud particle effective radius and thermodynamic phase. J. Geophys. Res. 113, D04208. doi:10.1029/2007JD008600.

Rossow, W.B., Schiffer, R.A., 1991. ISCCP cloud data products. Bull. Am. Meteorol. Soc. 72, 2–20.

Rossow, W.B., Schiffer, R.A., 1999. Advances in understanding clouds from ISCCP. Bull. Am. Meteorol. Soc. 80, 2261–2287.

Rossow, W.B., Mosher, F., Kinsella, E., Arking, A., Desbois, M., Harrison, E., Minnis, P., Ruprecht, E., Seze, G., Simmer, C., Smith, E., 1985. ISCCP cloud algorithm intercomparison. J. Climate Appl. Meteorol. 24, 877–903.

Schmetz, J., Pili, P., Tjemkes, S., Just, D., Kerkmann, J., Rota, S., Ratier, A., 2002. An introduction to Meteosat Second Generation (MSG). Bull. Am. Meteorol. Soc. 83, 977–992.

Schreiber, W.E., 1986. Case study of thunderstorms initiated by radar-observed convergence lines. Mon. Weather Rev. 114, 2256–2266.

Siewert, C.W., Koenig, M., Mecikalski, J.R., 2010. Application of Meteosat Second Generation data towards improving the nowcasting of convective initiation. Meteorol. Appl. 17, 442–451.

Smith Jr., W.L., Minnis, P., Young, D.F., 2000. An icing product derived from operational satellite data. Proc. AMS 9th Conf. Aviation, Range, and Aerospace Meteorol., Orlando, FL, pp. 256–259. 11–15 Sept.

Smith Jr., W.L., Minnis, P., Bernstein, B.C., Rapp, A.D., Heck, P.W., 2002. Supercooled liquid water cloud properties derived from GOES: Comparisons with in situ aircraft measurements. 10th AMS Conf. Aviation, Range, and Aerospace Meteorol., Portland, OR, pp. 89–92. May 13–16.

Smith Jr., W.L., Minnis, P., Bernstein, B.C., McDonough, F., Khaiyer, M.M., 2003. Comparison of supercooled liquid water cloud properties derived from satellite and aircraft measurements. Proc. FAA In-Flight Icing/De-icing International Conference, Chicago, IL. June 16–20, CD_ROM, 2003-01-2156.

Smith Jr., W.L., Minnis, P., Finney, H., Palikonda, R., Khaiyer, M.M., 2008. An evaluation of operational GOES-derived single-layer cloud top heights with ARSCL data over the ARM Southern Great Plains Site. Geophys. Res. Lett. 35, L13820. doi:10.1029/2008GL034275.

Strabala, K.I., Ackerman, S.A., Menzel, W.P., 1994. Cloud properties inferred from 8–12 μm data. J. Appl. Meteorol. 33, 212–229.

Watts, P.D., Mutlow, C.T., Baran, A.J., Zavody, A.M., 1998. Study on Cloud Properties derived from Meteosat Second Generation Observations. EUMETSAT ITT no. 97/181. Final Report. 344 pp. [Available from EUMETSAT, Am Kavalleriesand 31, D-64295 Darmstadt, Germany.].

Weygandt, S., Minnis, P., Benjamin, S.G., Devenyi, D., Brown, J.M., 2006. Cloud and hydrometeor analysis using metar, radar, and satellite data within the RUC/Rapid-Refresh model. Proc. AMS 12th Conf. Aviation Range and Aerospace Meteorol., Atlanta, GA. 29 Jan. – 2 Feb. 2006.

Wilks, D.S., 2006. Statistical Methods in the Atmospheric Sciences, 2nd ed. Academic Press. 627 pp.

Wilson, J.W., Mueller, C.K., 1993. Nowcasts of thunderstorm initiation and evolution. Weather Forecast. 8, 113–131.

Wolfson, M.M., Clark, D.A., 2006. Advanced Aviation Weather Forecasts. MIT Linc. Lab. J. 16 (Number 1).

Wulfmeyer, V., Behrendt, A., Bauer, H.S., Kottmeier, C., Corsmeier, U., Blyth, A., Craig, G., Schumann, U., Hagen, M., Crewell, S., Di Girolamo, P., Flamant, C., Miller, M., Montani, A., Mobbs, S., Richard, E., Rotach, M.W., Arpagaus, M., Russchenberg, H., Schlüssel, P., König, M., Gärtner, V., Steinacker, R., Dorninger, M., Turner, D.D., Weckwerth, T., Hense, A., Simmer, C., 2008. RESEARCH CAMPAIGN: The Convective and Orographically Induced Precipitation Study. Bull. Am. Meteorol. Soc. 89, 1477–1486.

Yuan, T., Li, Z., Zhang, R., Fan, J., 2008. Increase of cloud droplet size with aerosol optical depth: An observation and modeling study. J. Geophys. Res. 113, D04201. doi:10.1029/2007JD008632.

Zhao, T.X.-P., Laszlo, I., Guo, W., Heidinger, A., Cao, C., Jelenak, A., Tarpley, D., Sullivan, J., 2008. Study of long-term trend in aerosol optical thickness observed from operational AVHRR satellite instrument. J. Geophys. Res. 113. doi:10.1029/2007JD009061.

Zinner, T., Mannstein, H., Tafferner, A., 2008. Cb-TRAM: Tracking and monitoring severe convection from onset over rapid development to mature phase using multi-channel Meteosat-8 SEVIRI data. Meteorol. Atmos. Phys.Spinger-Verlag. doi:10.1007/s00703-008-0290-y.